Small-scale electron density and magnetic-field structures in the wake of an ultraintense laser pulse

T. V. Liseikina,[1,2] F. Califano,[3] V. A. Vshivkov,[1,2] F. Pegoraro,[4] and S. V. Bulanov[5,6]
[1]*Forum of Theoretical Physics, INFM, Pisa, Italy*
[2]*Institute of Computational Technologies, SD RAS, Novosibirsk, Russia*
[3]*Dipartimento di Astronomia, Università di Firenze and INFM, Sezione A, Pisa, Italy*
[4]*Department of Physics, Pisa University and INFM, Sezione A, Pisa, Italy*
[5]*Scuola Normale Superiore, Pisa, Italy*
[6]*General Physics Institute, RAS, Moscow, Russia*
(Received 7 December 1998)

We investigate the interaction of a high intensity ultrashort laser pulse with an underdense collisionless plasma in the regime where the Langmuir wake wave excited behind the laser pulse is loaded by fast particle beams, formed during the wake wave breaking. The beam loading causes the deterioration of the central part of the wake wave near the pulse axis, and the formation of bunches of sharply focalized ultrarelativistic electrons. The bunches of electrons generate a fast propagating magnetic field, which we interpret in terms of the magnetic component of the Lienard-Wiechert potential of a moving electric charge.
[S1063-651X(99)06611-8]

PACS number(s): 52.40.Nk, 52.60.+h, 52.65.Rr, 41.20.−q

I. INTRODUCTION

The problem of the generation of quasistatic magnetic fields by laser pulses in plasmas is one of the most important in the physics of the interaction of ultraintense electromagnetic radiation with plasmas, because of its influence on the transport processes and on the focalization of fast particles in the laser wake field accelerator [1] and in the fast ignition scheme [2] in inertial fusion. Theoretical studies predict large self-generated magnetic fields with magnitudes that can reach several hundreds MG or even 10^{10} G, and are localized in a region with a transverse size of the order of several tens of μm and with a macroscopic length [3,4]. This provides the source for the largest quasistationary magnetic fields under Earth conditions. Recent observations of a quasistatic magnetic field in the MG range generated by a relativistically intense laser pulse in a plasma was reported in Ref. [5].

In these relativistic regimes the most plausible mechanism of magnetic field generation is associated with the electric current produced by the electrons accelerated inside the self-focusing channel of the laser pulse [3] by the strong electric fields that arise at the wave break of the wake plasma waves. Plasma quasineutrality requires that the fast-electron current be canceled by a cold electron current of opposite sign. These oppositely directed currents repel each other. This repulsion and the consequent growth of the magnetic field are manifestations of the electric current filamentation instability [6], which is similar to the well known Weibel instability [7] that occurs in plasmas with anisotropic distribution functions. This mechanism of magnetic field generation was discussed in detail in several papers [3,6–8] and will be shown also to be at work in the simulation results presented in the present paper. In addition, it will be shown that such fast electron currents may be responsible for the inverted curvature of the Langmuir wake waves observed in these simulations in the region far from the laser pulse. However, conditions can be realized where a highly focalized bunch of fast electrons is formed with a local density much larger than that of the cold electrons. In such a regime the reverse electric current carried by the cold electrons may not be sufficient to neutralize both the electric current and the charge of the bunch. In this case a magnetic field is seen in the numerical simulations, propagating in the laboratory frame with the fast electron bunch. This magnetic field can be described in terms the Lienard-Wiechert potentials of a moving electric charge, and corresponds to the Lorentz transformed electrostatic field generated by the electron bunch in the comoving reference frame.

The generation of high current relativistic beams and hot electrons by high-power, short laser pulses propagating in underdense and overdense plasmas, respectively, was also investigated in two recent papers [9,10] that appeared in press after the submission of the present work. In particular, in Ref. [9] it was shown with the help of two-dimensional (2D) particle-in-cell (PIC) simulations that in an underdense plasma electron self-trapping and acceleration from the wave breaking of the plasma waves in the wake of the pulse lead to effective particle acceleration (as discussed previously in Ref. [11]) and to the formation of multiple electron bunches. Wave breaking also causes an increase of the effective phase velocity of the wake field. The injection of electrons into the acceleration phase of the wake wave by exploiting the break of the wake wave that occurs in an inhomogeneous plasma due to the change of the Langmuir frequency was analyzed in Ref. [12] in a 1D geometry, together with the effect of beam loading on the structure of the wake field.

In the present paper we address the dynamics and the spatial focalization of relativistic electron bunches produced by wave breaking, and discuss the effect on the shape of the bunch of relativistic oscillations due to the transverse electric field. In addition, we investigate explicitly the nature of the electromagnetic fields that such ultrarelativistic bunches create. These Lienard-Wiechert fields are of interest both be-

cause they arise from a fundamental process of relativistic electrodynamics and because they are essentially transverse fields with features that closely resemble those of a subcycle laser pulse. Subcycle laser pulses were considered recently [13,14] with the aim of exploiting a nonadiabatic mechanism of charged particle acceleration.

II. MAGNETIC FIELD PATTERNS

We expect different patterns of magnetic field to be generated in a plasma depending on whether they are produced by a wide electron beam, as in the case examined in Ref. [3], or by a highly focalized bunch of ultrarelativistic electrons. This difference is seen in the 2D PIC simulations we performed using the fully relativistic code described in Ref. [15] in laser-plasma regimes where the Langmuir wake wave excited behind the laser pulse is loaded by fast electrons formed during the wake wave breaking. In these simulations the length (in the longitudinal direction along x) of the computational region is 160λ, and its width (in the transverse direction along y) is 90λ. The cell size is $(0.125\times 0.125)\lambda^2$. The total number of particles is approximately 10^7. The plasma begins at $x=0$ and is preceded by a vacuum region 5λ long. The laser pulse is initialized outside the plasma in the vacuum region $x<0$. A pulse with dimensionless amplitude $a=2.5$ propagates in an underdense plasma with $\omega/\omega_p=10$. The pulse is s polarized (i.e., the components of the electromagnetic fields of the pulse in the vacuum region are B_x, B_y, and E_z) and its width and length are 30λ and 8λ, respectively.

Figure 1 shows the spatial structures of the electron density (a), the quasistatic magnetic field B_z (b), and the y component of the electric field (c) in the (x,y) plane at $t=120$. Here and below time and lengths are normalized on $2\pi/\omega$ and λ, respectively. In frame (a) we see that in the interval $50<x<100$ there are six maxima that correspond to the modulation of the electron density in the wake wave. The width of the wake field region is about 40λ, and the wake wavelength is $\approx 10\lambda=(\omega/\omega_p)\lambda$. In the leading part just behind the laser pulse an electron bunch is localized in the regions $x\approx 103$ and $y\approx 0$. The secondary wake wave excited by the bunch in the region $-5<y<5$ distorts the primary wake field pattern, producing a strong modulation of the electron density in the transverse direction. An analogous effect is seen in the 2D simulations reported in Ref. [9] [see, e.g., Fig. 4(c)], where the electron beam is found to act as an additional source for the wake field.

We see that the curvature of the constant phase surfaces of the wake wave corresponding to the density maxima furthest from the laser pulse is opposite to that which was discussed in Ref. [16] and which is seen in the unspoiled outer part of the first and second density maxima after the laser pulse in frame (a). A similar inverted curvature was observed recently in finite-difference 2D ''Vlasov'' simulations of the interaction of a high amplitude laser pulse with a finite temperature plasma. Each feature in the electron density finds its counterpart in the magnetic field pattern presented in frame (b) and in the y component of the electric field in frame (c). In frame (b) we see a periodic modulation along the x axis of the z component of the magnetic field with the period of the wake field. However, the mechanism of the magnetic field

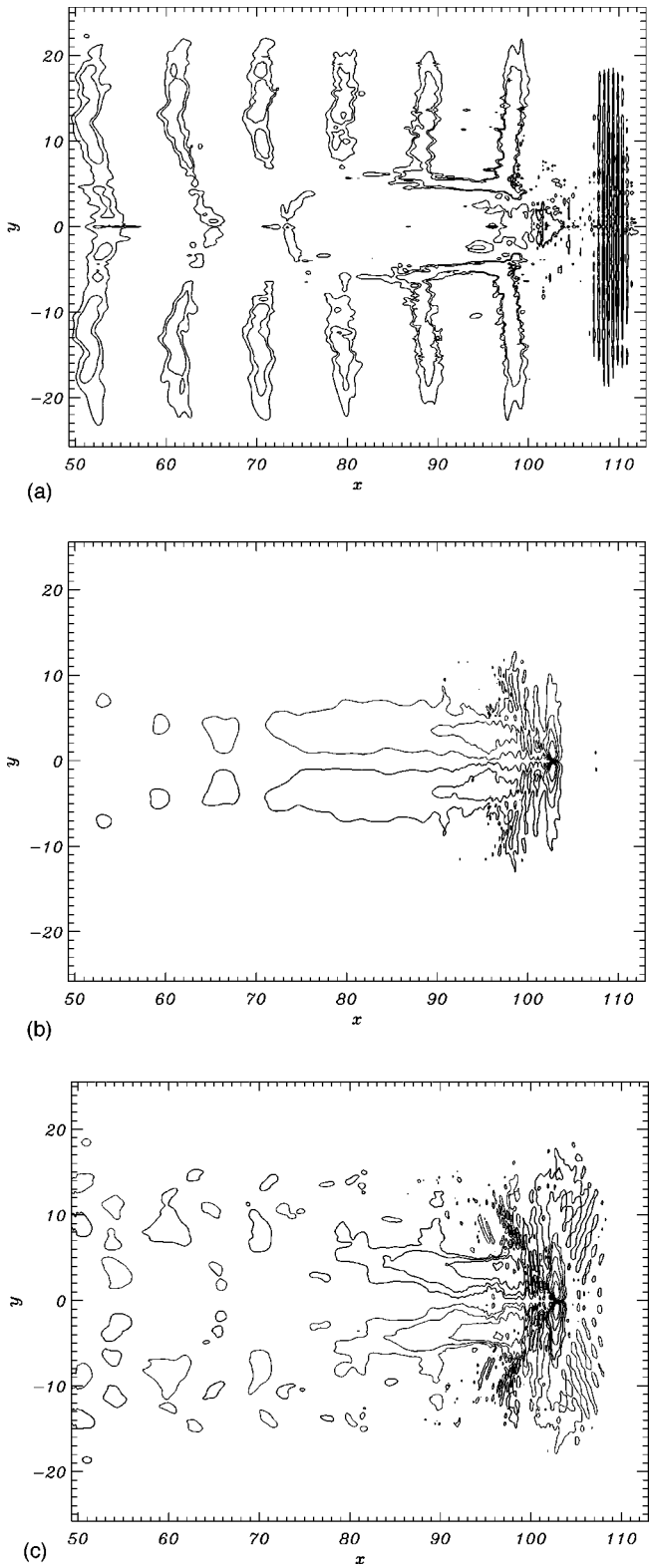

FIG. 1. Distribution of the electron density (a) of the z component of the magnetic field (b) and of the y component of the electric field (c) in the (x,y) plane behind the laser pulse at $t=120$.

generation cannot be simply attributed to the current driven by the nonlinear plasma wave [4], because the sign of the magnetic field alternates in the transverse direction both above and below the pulse axis along the wake wave. The absolute value of the magnetic field in the wake is ≈ 0.08. In

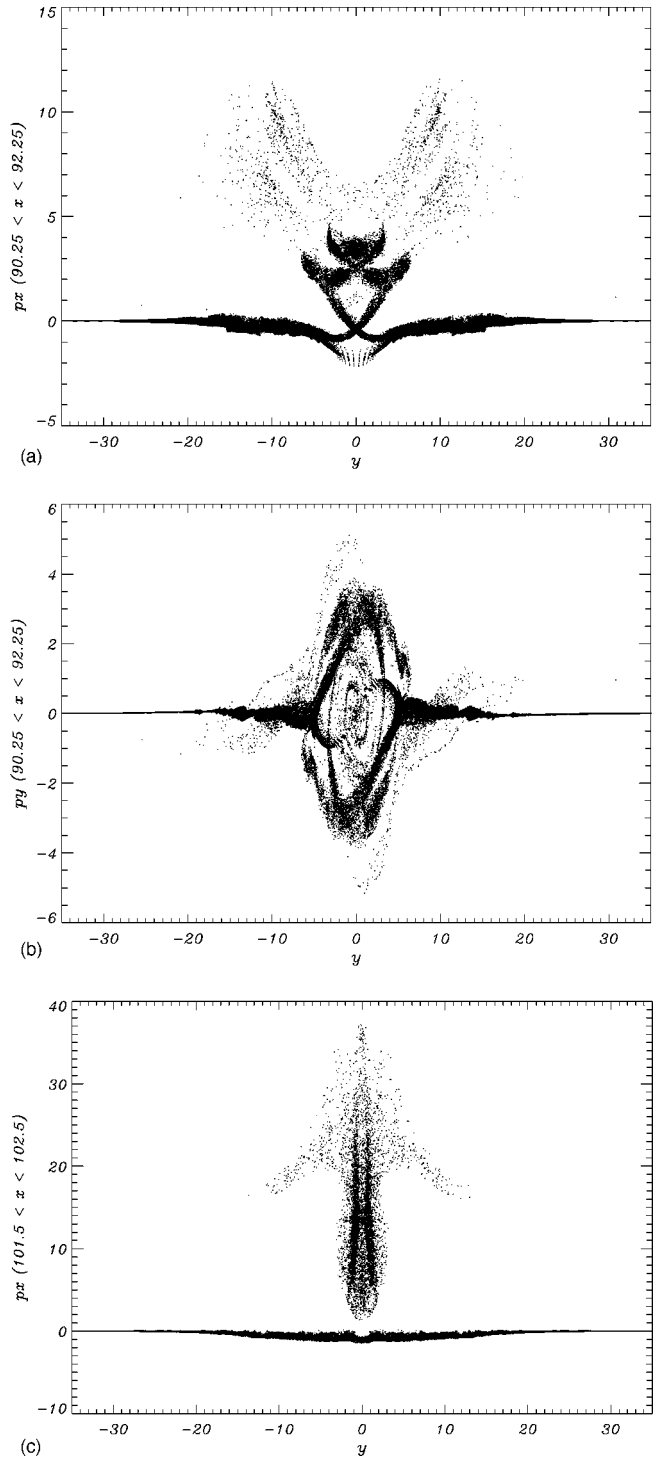

FIG. 2. Phase planes (p_x,y) (a) and (p_y,y) (b) at $x\approx 92$ and (p_x,y) at $x\approx 102$ (c) for $t=120$. Momenta are normalized on $m_e c$.

this region a wide beam of fast electrons is present, as seen in Figs. 2(a) and 2(b) where the (p_x,y) and (p_y,y) phase planes at $x\approx 92$ are shown, and the magnetic field generation can be interpreted as due to the filamentation instability of the electric current. The fast electrons produced by the wake wave breaking create an effectively anisotropic momentum distribution. Under such conditions the plasma is unstable against the excitation of an electromagnetic-type instability, which leads to the filamentation of electric currents carried by the fast electrons and by the electrons of the cold plasma

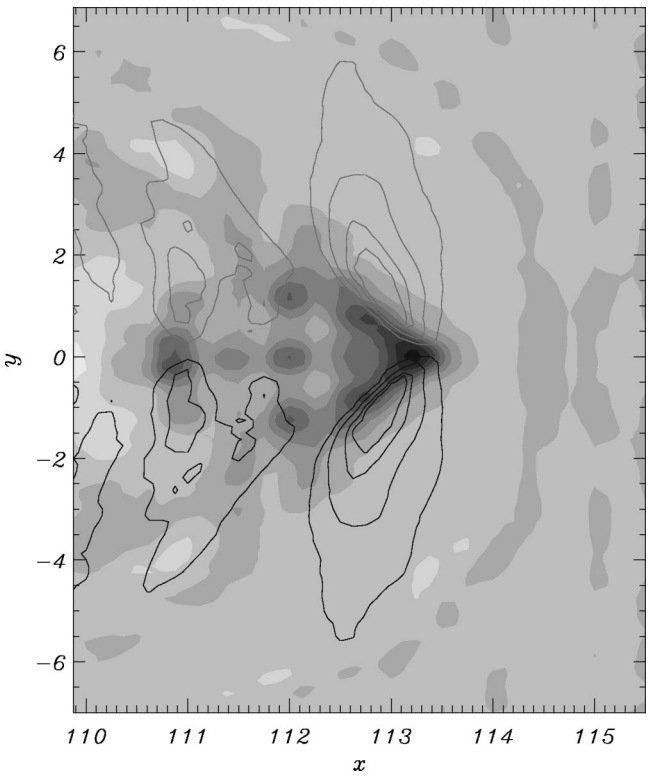

FIG. 3. Enlargement of the electron bunch region at $t=130$. The electron density (shaded plot) and the z component of the magnetic field are shown.

component [6,7]. This in turn results in alternate magnetic polarities. The scale of the magnetic field inhomogeneity is $(2-3)\lambda$ which corresponds to a wave number of the filamentation instability $k_b\approx\pi/\lambda=\omega/(2-3)c>k_p=\omega_p/c$. We find that k_b/k_p is about 3. In this limit, in the relativistic particle regime, the instability growth rate is of order of ω_p.

III. LIENARD-WIECHERT POTENTIALS

In Fig. 1(b), in the leading part of the wake, we see a region with a very strong magnetic field (≈ 0.24) in the z direction, with opposite signs in the upper and lower half-planes. A similar feature is seen in Fig. 1(c) in the y component of the electric field. Both the magnetic and electric fields are localized in a narrow domain elongated in the transverse direction. The location along x of these electromagnetic fields coincides with the location of the sharp electron bunch seen in Fig. 1(a) at $x\approx 103$. An enlarged picture of the electron density and the z component of the magnetic field in the bunch region (at $t=130$) is shown in Fig. 3.

The elongation in the x direction of the electron bunch is due to the relativistic motion of the electrons in the inhomogeneous (in the transverse direction) wake field excited behind a laser pulse of finite width S. Close to the pulse axis we approximate the electrostatic potential of the wake wave as

$$\varphi(x,y,t)=\varphi_m(1-y^2/S^2)\sin[\psi(x,y)], \tag{1}$$

with $\psi(x,y)=\omega_p(y)(t-x/v_{\rm ph})$, the Langmuir frequency $\omega_p(y)$ depends on y as $\omega_p(y)=\omega_p(0)+\Delta\omega_p(y/S)^2$, and $v_{\rm ph}$ is the phase velocity of the wake wave (see Ref. [8]).

We consider distances along x short compared to the particle acceleration length, so that the electrons in the bunch, which move along x essentially at the speed of light, keep their phase ψ_*, relative to the wake wave at $y=0$, constant. The value of ψ_* is taken so as to correspond to acceleration in the longitudinal direction and to focusing toward the axis. Calculating the x and the y components of the electric field, we obtain the equations of motion of a relativistic electron:

$$\dot{p}_x = -eE_x\left(1-\frac{\delta y^2}{S^2}\right), \tag{2}$$

$$\dot{p}_y = -e\left(\frac{E_y}{S}\right)y. \tag{3}$$

Here $E_x=\varphi_m(\omega_p(0)/v_{\rm ph})\cos(\psi_*)$, $\delta=[1-\Delta\omega_p/\omega_p(0)(1-\psi_*)\tan(\psi_*)]$ and $E_y=\varphi_m(2/S)[\sin(\psi_*)-(\Delta\omega_p/\omega_p(0))\psi_*\cos(\psi_*)]$. Assuming $y/S\ll 1$ and taking for the sake of simplicity, the longitudinal momentum p_x at $t=t_1$ independent of y and equal to $-eE_xt_1$, we obtain

$$p_x \approx -eE_x\left(t-\frac{\delta}{S^2}\int_{t_1}^{t} y^2 dt\right), \tag{4}$$

$$y \approx y_0\left(\frac{t_1}{t}\right)^{1/4}\cos\left(2\left(\frac{E_y c(t-t_1)}{E_x S}\right)^{1/2}\right), \tag{5}$$

where $t\gg E_xS/E_yc$, $p_x\gg m_ec$, and y_0 is the electron coordinate along y at $t=t_1$. We see that the longitudinal momentum p_x depends on the transverse coordinate y, in agreement with the phase space results shown in Fig. 2(c), and that the electrons oscillate along y with period $2\pi(tE_xS/E_yc)^{1/2}$. From these expressions it follows that the square of the transverse size of the electron bunch, averaged over the transverse oscillations, decreases as $y^2\approx y_0^2(t_1/t)^{1/2}$ while the longitudinal coordinate is given by

$$x \approx x_0 + c(t-t_1) + \frac{y^2-y_0^2}{2}\frac{E_y}{E_xS} + ct_1\left(\frac{mc}{eE_xt_1}\right)^2 \times\left(\frac{t_1}{2t}-\frac{1}{2}+\delta\frac{y_0^2}{S^2}\left(\frac{2}{3}\frac{t_1^{3/2}}{t^{3/2}}-\frac{t_1^2}{2t^2}-\frac{1}{6}\right)\right), \tag{6}$$

where, if oscillatory terms are disregarded, y_0^2 can be expressed as $y^2(t/t_1)^{1/2}$. The dependence of x on y in Eq. (6) is parabolic, and arises from two different contributions with different time dependences. The first contribution, proportional to $E_yc/2cE_xS$, arises from the square of the transverse momentum in the Lorentz factor in the relationship between the momentum and the velocity along x (electrons with smaller transverse oscillations are effectively lighter), while the second term, proportional to δ, arises from the transverse dependence of the force along x in Eq. (2). For $\delta>0$ and large t, both terms are negative. Computing the Jacobian $J=|\partial(x_0,y_0)/\partial(x,y)|$ of the transformation from the x_0 and y_0 coordinates to x and y, we find that the electron density in the bunch $n(x,y,t)=n(x_0,y_0)J$ increases asymptotically as $t^{1/4}$. Referring for simplicity to the first term only in Eq. (6), we find that, if at $t=t_1$ the contours of equal density inside the electron bunch are given by $x_0^2+y_0^2=$const, the shape of the bunch is given at $t\gg t_1$ by

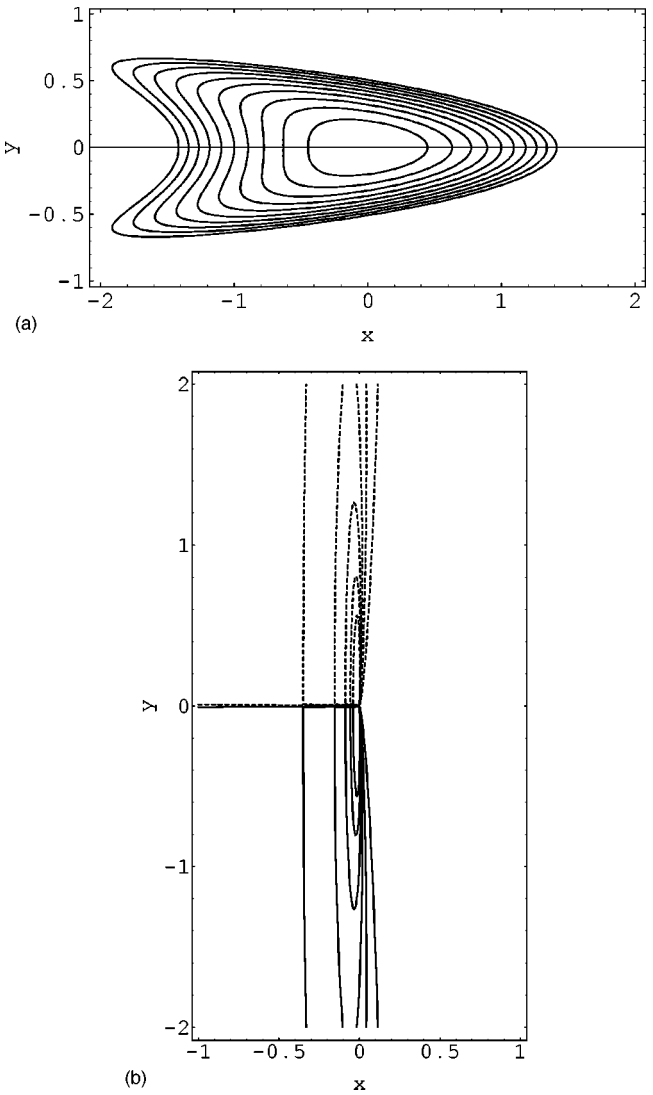

FIG. 4. Shape of the density of the bunch of fast electrons (a) as described by Eq. (7). (b) Magnetic field in the neighborhood of the tip of the fast electron bunch of electrons as obtained from Eq. (13).

$$\left[x-ct+y^2\left(\frac{t}{t_1}\right)^{1/2}\left(\frac{E_y}{2SE_x}\right)\right]^2+y^2\left(\frac{t}{t_1}\right)^{1/2}\approx\text{const}, \tag{7}$$

as illustrated in Fig. 4(a). The bunch of fast electrons has the form of a pointed arrow with its leading part described by

$$X \approx -y^2\left(\frac{t}{t_1}\right)^{1/2}\left(\frac{E_y}{2SE_x}+\frac{1}{2(x_0^2+y_0^2)^{1/2}}\right), \tag{8}$$

where X is the distance from the tip of the arrow. As $t\to\infty$, the front becomes narrower. In the Lorentz boosted frame with velocity V_x, where the electron bunch is instantaneously at rest, $p_x'=0$, (a prime indicates quantities in the boosted frame) the arrow is sharper. The Lorentz transformation to the boosted frame gives $y'=y$ and $x'=\gamma(x-V_xt)\approx(x-ct)|p_x|/(mc)\approx(x-ct)(eE_xt/mc)$, where $\gamma\approx|p_x|/(mc)$ is the Lorentz factor. Thus Eq. (8) becomes

$$x' \approx -y'^2 \left(\frac{t}{t_1}\right)^{1/2} \left(\frac{eE_x t}{mc}\right) \left(\frac{E_y}{2SE_x} + \frac{1}{2(x_0^2+y_0^2)^{1/2}}\right). \quad (9)$$

In the boosted frame the fast electron density decreases with time as $t^{-3/4}$, where t is the time measured in the laboratory frame.

The properties of the electric and magnetic fields of the electron bunch can be explained in terms of the Lienard-Wiechert potentials of the moving electron bunch [17]. As an illustration, we shall discuss a model distribution corresponding the limit of a needlelike (equipotential) electron density which corresponds to the asymptotic limit $t \to \infty$. In this case, in the boosted frame the electrostatic potential can be written as [18]

$$\varphi' = \mathcal{C}\left(\frac{r'-x'}{2}\right)^{1/2}, \quad (10)$$

where $r' = (x'^2+y'^2)^{1/2}$, and $\mathcal{C}$ is a proportionality factor, related to the density in the electron bunch, that decreases with time (as measured in the laboratory frame) as $t^{-3/4}$. The potential φ' has a branch cut in the complex plane $x'+iy'$ along the positive x' axis corresponding to the position of the needle shaped bunch. The Lienard-Wiechert potentials of the moving bunch in the laboratory frame are obtained by a Lorentz transformation of φ' in Eq. (10),

$$\varphi \approx \gamma \mathcal{C}\left[\frac{(\gamma^2(x-ct)^2+y^2)^{1/2} - \gamma(x-ct)}{2}\right]^{1/2}, \quad (11)$$

and $\mathbf{A} \equiv \mathbf{A}\mathbf{e_x}$ with

$$A \approx -c\gamma \mathcal{C}\left[\frac{(\gamma^2(x-ct)^2+y^2)^{1/2} - \gamma(x-ct)}{2}\right]^{1/2}, \quad (12)$$

where $\mathbf{e_x}$ is the unit vector in the x direction. Then the z component of the magnetic field $B_z = -\partial_y A$ is approximately given by

$$B_z \approx \gamma \mathcal{C} \frac{cy}{\{8(\gamma^2(x-ct)^2+y^2)[(\gamma^2(x-ct)^2+y^2)^{1/2} - \gamma(x-vt)]\}^{1/2}}, \quad (13)$$

where $\gamma \approx eE_x t/mc$. The coefficient $\gamma\mathcal{C}$ in front of the potentials increases with time as $t^{1/4}$, in agreement with the behavior of the density in the laboratory frame. The magnetic field has opposite polarities in the upper plane and in the lower half-plane and, as a consequence of the simplified model adopted, tends to infinity at the origin as $\approx r^{-1/2}$. The region with the strong magnetic field is very narrow ($\Delta x \approx y/\gamma$) in the x direction, and elongated along y. The y component of the electric fields has approximately the same magnitude and the same spatial pattern. The contours of the z component of the magnetic field, which coincide with those of the y component of the electric field $-\partial_y \varphi$, obtained from Eq. (13), are plotted in Fig. 4(b) and correspond to those shown in Fig. 3, where we show the local structure of the electron density in the bunch and of the magnetic field as obtained from the PIC simulation reported in Fig. 1. In these calculations we have neglected the screening of the plasma on the electromagnetic fields generated by the electron bunch. This can be justified on the grounds that in the laboratory frame the fields arising from the Lienard-Wiechert potential generated by the short relativistic electron bunch are similar to those of an electromagnetic wave with a frequency higher than the local plasma frequency.

These results can be generalized to a 3D configuration. In this case the ''arrow'' has the form of a pointed paraboloid. The contraction of the electron trajectories toward the x axis (which is a consequence of the relativistic increase of their effective mass as their momentum along x increases) can be easily shown by referring to the following 3D equations of motion

$$\dot{\mathbf{p}} = -e\begin{pmatrix} E \\ 0 \\ 0 \end{pmatrix} - e\begin{pmatrix} 0 & -h_y v_y/c & -h_z v_z/c \\ 0 & \alpha_{yy}+h_y v_x/c & \alpha_{zy} \\ 0 & \alpha_{zy} & \alpha_{zz}+h_z v_x/c \end{pmatrix} \begin{pmatrix} x \\ y \\ z \end{pmatrix}. \quad (14)$$

These equations include the accelerating electric field $-E$ along the x axis, the effect of an azimuthal magnetic field $\mathbf{B} = \nabla \times \mathbf{A} = \nabla \times [(h_y y^2 + h_z z^2)/2]\mathbf{e}_x$, which vanishes at the x axis and represents the quasi static magnetic field, and of a transverse electric field, with an elliptic null along this axis, described by the potential $\varphi = -(\alpha_{yy} y y^2 + \alpha_{zz} z z^2)/2 - \alpha_{zy} yz$, with $\alpha_{yy} + \alpha_{zz} > 0$ and $\alpha_{yy}\alpha_{zz} - \alpha_{zy}^2 > 0$. Diagonalizing the symmetric y-z minor of the matrix in Eq. (14) along its principal axes, we recover along each principal direction a time behavior of the electron motion of the type given by Eq. (5). This is shown in Fig. 5 for $h_y = 1$, $h_z = 0.5$, $\alpha_{yy} = 0.75$, $\alpha_{zy} = 0.25$, and $\alpha_{zz} = 0.75$. In frame (a) we show the electron acceleration along x, in frame (b) the transverse electron motion, in frame (c) the contraction of the transverse orbit size, measured by $y^2(t) + z^2(t)$, as a function of $x(t)$; and in frame (c) the electron trajectory in (p_y, y) phase space. Notice the resemblance between this frame and the PIC result shown in Fig. 2(b). In addition, notice the increase of p_y as y decreases, which is related to the conservation of the adiabatic invariants along the principal axes of oscillation. Finally, note the similarity between the accelerated orbit shown in Fig. 5(a) and the electron orbit inside the channel behind the laser pulse shown in Fig. 7(a) of Ref. [10]. The latter orbit is obtained by tracking in time a specific particle in a 2D PIC simulation.

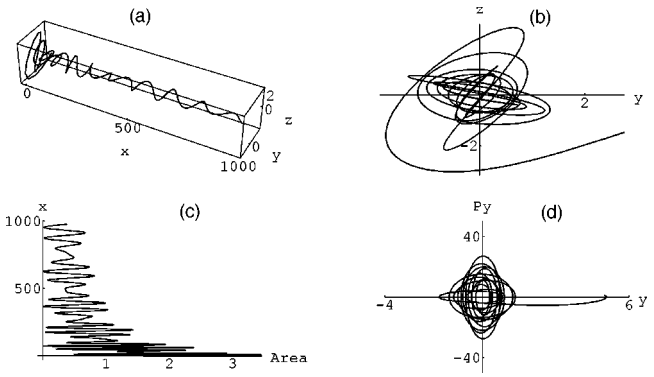

FIG. 5. 3D motion (a) of an electron accelerated along x in the transverse electric and magnetic fields given by Eq. (14). (b) Transverse motion. (c) Contraction of the transverse area of the electron trajectory $y^2(t)+z^2(t)$ as a function of $x(t)$. (d) Electron trajectory in (p_y, y) phase space.

Extending the 2D treatment given before, we compute the Lienard-Wiechert fields in a 3D configuration near the vertex of an (infinitely) sharp paraboloid. In the boosted frame where the fast electron bunch is at rest, we find

$$\varphi' = \mathcal{D}\,\ln|\rho' - x'|, \tag{15}$$

where $\rho' = (x'^2 + y'^2 + z'^2)$, and the proportionality factor $\mathcal{D}$ depends on time as $t^{-1/2}$. Calculating the Lienard-Wiechert potentials of the moving bunch in the laboratory frame we find that the magnetic field is azimuthal, the electric field is radial in the plane perpendicular to the laser pulse axis, and both fields are proportional to ρ^{-1} near the paraboloid vertex. In this case the potentials in the laboratory frame increase with time as $t^{1/2}$, as follows from the stronger focalization of the electron bunch in a 3D configuration.

IV. INVERTED CURVATURE

In Fig. 1(a) we see that near the axis the curvature of the constant phase surfaces in the wake wave furthest from the laser pulse is opposite to that of the ''horseshoe'' structures discussed in Refs. [8] and [16]. In this latter case the curvature of the constant phase surfaces was associated with the increase of the Langmuir frequency with the transverse coordinate, away from the laser pulse axis, due to electron density inhomogeneities and/or to relativistic effects of the electron mass. The ''inverted'' curvature of the wake wave fronts in Fig. 1(a) may be interpreted as due to kinetic effects. Similarly to the case of a finite electron temperature plasma, the dispersion equation of Langmuir waves changes [19] in the presence of a sufficiently high density of fast electrons and the real part of its frequency ω_L is given by

$$\omega_L^2(k) \approx \omega_p^2(\mathcal{E}) + \alpha(\mathcal{E})k^2c^2. \tag{16}$$

Here $\mathcal{E}$ is the effective energy of the fast electrons. The specific form of the functions $\omega_p(\mathcal{E})$ and $\alpha(\mathcal{E})$ depends on the particle distribution in phase space. In the nonrelativistic limit, when the particle distribution is Maxwellian with temperature T, $\omega_p(\mathcal{E}) = \omega_p$ and $\alpha(\mathcal{E}) = 3T/(mc^2)$, while in the ultrarelativistic case [for an isotropic distribution with $T = \mathcal{E}/3$] $\omega_p(\mathcal{E}) = (m/\mathcal{E})^{1/2}\omega_p$ and $\alpha(\mathcal{E}) = 3/5$. If we apply the dispersion relation (16) to the resonance condition $\omega_L(k) = kv_g$ between the frequency ω_L of the wake wave and the group velocity v_g of the laser pulse we obtain $k \approx \omega_p/v_g + \alpha(\mathcal{E})\omega_p^2/(2v_g^3)$ which shows that the wave number of the wake field is larger in the region where $\alpha(\mathcal{E})$ is larger. If the effective temperature is inhomogeneous in the transverse direction and has its maximum at the laser pulse axis, the wavelength of the wake wave is shorter on the axis and increases outwards. This transverse dependence of the wake wave number is opposite to that which leads to the horseshoe structure, and leads to wake fronts with ''inverted'' curvature.

In addition, at a distance from the laser pulse larger than $\approx S v_g^2/(2\alpha\omega_p)$, where S is the pulse width, the effects of the Langmuir wave propagation in the transverse direction become important. This transverse propagation is again due to kinetic effects and occurs at the group velocity $v_{Lg} \approx \alpha\omega_p c^2/v_g$ as follows from Eq. (16). In order to describe the wave pattern in the wake we use the approach developed in Ref. [20]. In the frame comoving with the laser pulse, the dispersion equation (16) can be rewritten as

$$k_x v_g = \omega_p + \tilde{\alpha} k_y^2, \tag{17}$$

where v_g is the group velocity of the laser pulse, $\tilde{\alpha} = \alpha c^2/2\omega_p$ and we assume $\tilde{\alpha}k_x^2 \ll \omega_p$. In the wake behind the laser pulse the wave vector is a function of the space coordinates. Following Ref. [20], we write the so called consistency relationship

$$\frac{\partial k_y}{\partial x} - \frac{\partial k_x}{\partial y} = 0. \tag{18}$$

The dispersion equation (17) gives the x component of the wave vector k_x as a function of k_y. Then Eq. (18) yields

$$\frac{\partial k_y}{\partial x} - \frac{2\tilde{\alpha}}{v_g} k_y \frac{\partial k_y}{\partial y} = 0. \tag{19}$$

Hence k_x and k_y are constant on the characteristics

$$\frac{dk_x}{dk_y} = -\frac{2\tilde{\alpha}}{v_g} k_y. \tag{20}$$

Now we assume that the size of the laser pulse is small compared with its distance from the point where we see the wake wave. This means that the source of the wake can be approximated as a point, and that the characteristics pass through the origin in coordinate space. As a result we have

$$\frac{y}{x} = -\frac{2\tilde{\alpha}}{v_g} k_y, \tag{21}$$

which gives $k_y = -(v_g/2\tilde{\alpha})(y/x)$, and $k_x = \omega_p/v_g + (v_g/4\tilde{\alpha})(y/x)^2$. The phase θ of the wave in the comoving frame does not depend on time and is equal to $\theta = k_x x + k_y y$. The position of the wake wave crests corresponds to constant values of the phase θ. We rewrite this expression as

$$\left(x-\frac{\theta v_g}{2\omega_p}\right)^2-\frac{v_g^2}{4\tilde{\alpha}\omega_p}y^2=\frac{\theta^2 v_g^2}{4\omega_p^2}. \tag{22}$$

This describes hyperbolae with ''inverted curvature.'' We see that the wake is localized inside a cone with angle ξ given by $\tan\xi=\sqrt{4\tilde{\alpha}\omega_p/v_g^2}$.

V. CONCLUSIONS

In this paper we have shown, with 2D PIC computer simulations, that a high intensity, ultrashort laser pulse interacting with an underdense plasma excites a strong magnetic field through at least two different mechanisms. The first mechanism corresponds to the nonlinear current filamentation instability of the fast electron beam produced by the break of the wake wave, while the second is associated with the Lienard-Wiechert potentials of a moving electron bunch. In contrast to previous analyses of the generation of a magnetic field by a laser pulse in a plasma in regimes where the electrons are relativistic, here we have studied the behavior of a laser pulse considerably wider than the inertial skin depth. The amplitude of the pulse was chosen sufficiently high and the plasma density sufficiently low in order to investigate the conditions where the wake wave excited behind the laser pulse is loaded by fast particle beams formed during the wake wave breaking, while the influence of the fast particles is not sufficient to destroy the wake wave completely. The second mechanism of the magnetic field generation is related to the fact that wave breaking produces sharply focalized bunches of ultrarelativistic electrons. In our simulations we see the strong magnetic field generated by the bunch. We explain this magnetic field in terms of the magnetic component of the Lienard-Wiechert potentials of a moving electric charge. To our knowledge these are the first detailed observations of Lienard-Wiechert fields in simulations of the interaction of a high intensity laser pulse with a plasma.

ACKNOWLEDGMENTS

Fruitful discussions with T. Esirkepov, N. Naumova, and H. Ruhl are greatly acknowledged, together with their critical analysis of the numerical results presented in this paper. We are pleased to acknowledge the Cineca supercomputing center of Bologna and the Scuola Normale Superiore of Pisa for the use of their Cray T3E and Origin 2000, respectively. Parts of the calculations were performed under an INFM research project at Cineca.

[1] T. Tajima and J. M. Dawson, Phys. Rev. Lett. **43**, 267 (1979).
[2] S. C. Wilks, J. M. Kruer, M. Tabak, and A. B. Langdon, Phys. Rev. Lett. **69**, 1383 (1992).
[3] G. A. Askar'yan, S. V. Bulanov, F. Pegoraro, and A. M. Pukhov, Pis'ma Zh. Éksp. Teor. Fiz. **60**, 240 (1994) [JETP Lett. **60**, 251 (1994)]; S. V. Bulanov, T. Zh. Esirkepov, M. Lontano, F. Pegoraro, and A. M. Pukhov, Phys. Rev. Lett. **76**, 3562 (1996).
[4] L. Gorbunov, P. Mora, and T. M. Antonsen, Jr., Phys. Rev. Lett. **76**, 2945 (1996); Z. M. Sheng, J. Meyer-ter-Vehn, and A. Pukhov, Phys. Plasmas **5**, 3764 (1998).
[5] M. Borghesi, A. J. Mackinnon, R. Gaillard, O. Willi, A. Pukhov, and J. Meyer-ter-Vehn, Phys. Rev. Lett. **80**, 5137 (1998).
[6] F. Califano, F. Pegoraro, and S. V. Bulanov, Phys. Rev. E **56**, 963 (1997); F. Califano, F. Pegoraro, S. V. Bulanov, and A. Mangeney, *ibid.* **57**, 7048 (1998).
[7] E. W. Weibel, Phys. Rev. Lett. **2**, 83 (1959); V. Yu. Bychenkov *et al.*, Zh. Éksp. Teor. Fiz. **98**, 1269 (1990) [Sov. Phys. JETP **71**, 709 (1990)]; F. Pegoraro, S. V. Bulanov, F. Califano, and M. Lontano, Phys. Scr. **T63**, 262 (1996).
[8] S. V. Bulanov, F. Pegoraro, A. M. Pukhov, and A. S. Sakharov, Phys. Rev. Lett. **78**, 4205 (1997).
[9] K.-C. Tsang, W. B. Mori, and T. Katsouleas, Phys. Plasmas **6**, 2105 (1999).
[10] B. F. Lasinski, A. B. Langdon, S. P. Hatchett, M. H. Key, and M. Tabak, Phys. Plasmas **6**, 2041 (1999).
[11] S. V. Bulanov, V. I. Kirsanov, and A. S. Sakharov, Pis'ma Zh. Éksp. Teor. Fiz. **53**, 540 (1991) [JETP Lett. **53**, 565 (1991)].
[12] S. V. Bulanov, N. Naumova, F. Pegoraro, and J. Sakai, Phys. Rev. E **58**, 5257 (1998).
[13] B. Rau, T. Tajima, and H. Hojo, Phys. Rev. Lett. **78**, 3310 (1987).
[14] K. Akimoto, Phys. Plasmas **4**, 3101 (1997).
[15] A. V. Vshivkov, N. M. Naumova, F. Pegoraro, and S. V. Bulanov, Phys. Plasmas **5**, 2727 (1998).
[16] S. V. Bulanov and A. S. Sakharov, Pis'ma Zh. Éksp. Teor. Fiz. **54**, 208 (1991) [JETP Lett. **54**, 203 (1991)]; S. V. Bulanov, F. Pegoraro, and A. M. Pukhov, Phys. Rev. Lett. **74**, 710 (1995).
[17] L. D. Landau and L. M. Lifshitz, *The Classical Theory of Fields* (Pergamon Press, Oxford, 1975).
[18] L. D. Landau and L. M. Lifshitz, *Electrodynamics of Continuous Media* (Pergamon Press, Oxford, 1984).
[19] V. P. Silin, Zh. Éksp. Teor. Fiz. **38**, 1577 (1960) [Sov. Phys. JETP **11**, 1136 (1960)]; F. Pegoraro and F. Porcelli, Phys. Fluids **27**, 1665 (1984).
[20] G. B. Whitham, *Linear and Nonlinear Waves* (Wiley, New York, 1974).